Journal of Alloys and Compounds 509 (2011) 8761–8769

Contents lists available at ScienceDirect

Journal of Alloys and Compounds

journal homepage: www.elsevier.com/locate/jallcom

Synthesis and optical properties of CuO nanostructures obtained via a novel thermal decomposition method

R. Al-Gaashani[a,b,*], S. Radiman[a], N. Tabet[c], A. Razak Daud[a]

[a] School of Applied Physics, Faculty Science and Technology, Universiti Kebangsaan Malaysia, 43600 Bangi, Selangor, Malaysia
[b] Department of Physics, Faculty of Applied Sciences, Thamar University, Dhamar, Republic of Yemen
[c] Department of Physics, and Center of Research Excellence in Nanotechnology, King Fahd University of Petroleum and Minerals, Dhahran, Saudi Arabia

ARTICLE INFO

Article history:
Received 8 March 2011
Received in revised form 17 May 2011
Accepted 14 June 2011
Available online 21 June 2011

Keywords:
CuO
Nanostructures
Thermal decomposition
Optical properties

ABSTRACT

We report a novel method that allows the synthesis of copper oxide (CuO) nanostructures and control their morphology and size by rapid thermal decomposition of copper nitrate (CuN_2O_6) under ambient conditions. The size and morphology of the nanostructures can be controlled by changing the temperature and the duration of the decomposition process. The structure of the products was investigated by X-ray diffraction (XRD), field emission scanning electron microscopy (FESEM) equipped with energy dispersive spectroscopy (EDS). The results showed that the morphology of the nanostructures changed as the temperature was varied and their size increased with increasing the treatment time. The optical properties of the samples were investigated by UV–vis spectroscopy and a photoluminescence (PL) spectrometer. Rice-like nanostructures were observed and analyzed by X-ray photoelectron spectroscopy (XPS)/EDS and XRD which confirmed that the as-synthesized powders correspond to pure CuO.

1. Introduction

Metal oxide semiconductors such as ZnO, TiO_2, WO_3, CdO, and CuO with their different nanostructures (particles, sheets, rods and wires) have attracted a great deal of attention from researchers in different fields because of their unique characteristics and various technological applications, including catalysis, ceramics, batteries, optics, photovoltaics, fuel cells, electrochromics, color pigments, coating technology, gas sensors, electronics, medical science and so on. Thus, metal oxide semiconductors are attracting significant attention of many researchers in different fields to develop new, cheap and effective methods to control and prepare metal oxide nanostructures [1–5].

CuO is an important p-type semiconductor oxide with a narrow band gap of about (1.2–1.4 eV) at room temperature [6,7]. In addition to the previous technological applications, CuO is particularly used as a fundamental material in high-Tc superconductors [8,9] and battery electrodes [10,11].

Up to date, several methods have been developed to synthesize CuO nanostructures, such as hydrothermal method [12], sol–gel [13] solid state reactions [14], precipitation technique [15], sonochemical route [16], microwave-assisted synthesis methods [17,18] and so on. A number of researchers have used thermal decomposition methods for the preparation of CuO nanostructures [19–21]. However, to the best of our knowledge, nobody used the new method described in this work. In addition, this new method is not limited to the synthesis of CuO nanostructures; it can be used for large-scale synthesis of other metal oxide nanostructures. In this work, we report a new method to synthesize and control nanostructured CuO with high purity. This technique involves the use of one-raw material without using any catalyst or template and one-step thermal decomposition of copper nitrate trihydrate to produce CuO nanostructures of significant amount. We have also investigated the effect of the preparation temperature and time on the size, structure, morphology and optical properties of CuO nanostructures.

2. Experimental

2.1. Samples preparation

CuO nanostructures were synthesized by one-step thermal decomposition of copper nitrate trihydrate ($CuN_2O_6{\cdot}3H_2O$) (Aldrich, Fluka) by conventional heating using a box oven. In a typical experiment, 1.3 g of copper nitrate trihydrate ($CuN_2O_6{\cdot}3H_2O$) was put inside a crucible. Then, the crucible was heated in a box oven at 300 °C for 20 min under ambient conditions. After the oven was switched off, the sample was quickly taken out of the oven. After cooling down to room temperature, it was observed that the green copper nitrate trihydrate was changed to a black

* Corresponding author at: School of Applied Physics, Faculty Science and Technology, Universiti Kebangsaan Malaysia, 43600 Bangi, Selangor, Malaysia.
Tel.: +60 173981135, fax: +60 389269470.
E-mail address: Rashad_jashani@yahoo.com (R. Al-Gaashani).

0925-8388/$ – see front matter © 2011 Elsevier B.V. All rights reserved.
doi:10.1016/j.jallcom.2011.06.056

Table 1
The crystallite size, the indirect and direct band gap of the CuO nanostructures synthesized at different temperatures.

Sample	Product	Morphology	Temperature (°C)/time (20 min)	Crystallite size (nm) (Scherrer)	Indirect bandgap E_g (eV)	Direct bandgap E_g (eV)
S1	CuO	Fish ribs-like	300	30.5	0.8	3.8
S3	CuO	Particles	600	43.6	0.95	3.7
S4	CuO	Particles	800	47.6	1.0	3.65

powder that was easily collected as it stuck very weakly to the bottom of the crucible. This sample was given the code (S1). The above experiment was repeated by changing the temperature which was set successively at 400 °C, 600 °C and 800 °C (see Table 1). Subsequently, a series of samples were prepared at T = 400 °C for different treatment times as shown in Table 2.

2.2. Characterization

The structural characterization of all samples was carried out by X-ray powder diffraction (XRD), using a Bruker-AXSD8 advance X-ray diffractometer with Cu-Kα radiation source (λ = 1.5418 Å). The size and morphology of the products were observed using a HITACHI S-4800 field emission scanning electron microscope (FESEM).

Sample prepared at 400 °C during 20 min has a nanorice-like structure (Fig. 2(c) and (d)). This sample was analyzed by X-ray photoelectron spectroscopy using XSAM-HS KRATOS electron spectrometer. X-ray source type MgK was used with 12 kV voltage and 10 mA current at 10^{-9} Torr pressure. The pass energy was set at 160 eV for the wide survey spectra and at 40 eV for the high resolution spectra of all elements of interest. Data processing was carried out using the Kratos software. The binding energies were corrected for the charge shift using the C 1s peak of graphitic carbon (BE = 284.6 eV) as reference.

The optical properties were measured by recording the (UV–vis) absorption and reflectance spectra at room temperature using a Perkin-Elmer Lambda 35 spectrophotometer in the 190–1100 nm wavelength range and a 10 mm quartz cuvette. The photoluminescence (PL) properties were investigated using Perkin Elmer LS55 Luminescence Spectrometer. The excitation wavelength was 250 nm.

3. Results and discussion

3.1. Structure and morphology of the products

3.1.1. Effect of temperature

Fig. 1 shows the XRD patterns of all samples prepared at 300 °C (S1), 400 °C (S2), 600 °C (S3) and 800 °C (S4) for 20 min treatments. The XRD patterns confirmed that all samples correspond to tenorite (CuO) composition, with a base-centered monoclinic structure (space group $C2/c$, a = 4.685 Å, b = 3.423 Å, c = 5.132 Å, $\alpha = \gamma = 90°$ and β = 99.52°; JCPDS card no. 41-0254).

The average crystallite sizes D (nm) of the as- prepared samples were estimated using Scherrer's formula [1]:

$$D = \frac{0.9\lambda}{\beta \cos\theta} \quad (1)$$

where λ is the X-ray wavelength of Cu-Kα radiation source (=0.15418 nm), β (in rad) is the full width at half maximum (FWHM) intensity of the diffraction peak located at 2θ, and θ is the Bragg angle. The average crystallite sizes of all samples were calculated as shown in Table 1. The results showed that the crystallite size

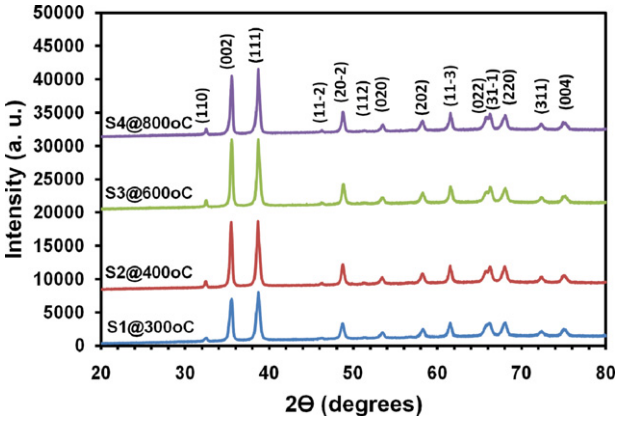

Fig. 1. XRD patterns of all samples prepared by thermal decomposition of copper nitrate during 20 min under atmospheric conditions at 300 °C (S1), 400 °C (S2), 600 °C (S3) and 800 °C (S4).

of the synthesized CuO nanostructures increased with increasing preparation temperatures (Table 1).

The thermal decomposition of copper nitrate under atmospheric conditions can be described as follows:

$$2Cu(NO_3)_2 \xrightarrow{\text{Rapid Heating (20 min)}} 2CuO + 4NO_2 \uparrow + O_2 \uparrow \quad (2)$$

Fig. 2 shows the FESEM images of the CuO samples synthesized at 300 °C (Fig. 2(a) and (b)), 400 °C (Fig. 2(c) and (d)), 600 °C (Fig. 2(e) and (f)) and 800 °C (Fig. 2(g) and (h)). The images show clearly the effect of changing temperatures on the size and morphology of the CuO nanostructures. The SEM images (Fig. 2(a) and (b)) show CuO nanostructures (fish ribs-like) with approximately 79 nm average width. Rice-like CuO nanostructures having about 80 nm average width and 250 nm length is shown in Fig. 2(c) and (d); however, Fig. 2(e)–(h) shows CuO nanoparticles that have non-uniform shape and size (about 180 nm average size). The sample prepared at 800 °C shows a tridimensional growth leading to the formation of compact polycrystalline structure of various grain sizes (Fig. 2(g) and (h)). It is clear that the morphology of the CuO nanostructures was changed by changing the temperature at a fixed treatment time.

Table 2
The crystallite size, the indirect and direct band gap of the CuO nanostructures synthesized during different times.

Sample	Product	Morphology	Time (min)/ temperature (400 °C)	Crystallite size (nm) (Scherrer)	Indirect bandgap E_g (eV)	Direct bandgap E_g(eV)
C10	CuO	Rice-like	10	28.5	0.5	3.5
S2	CuO	Rice-like	20	34.2	0.6	3.2
C1h	CuO	Rice-like	60	41.8	1.1	3.18

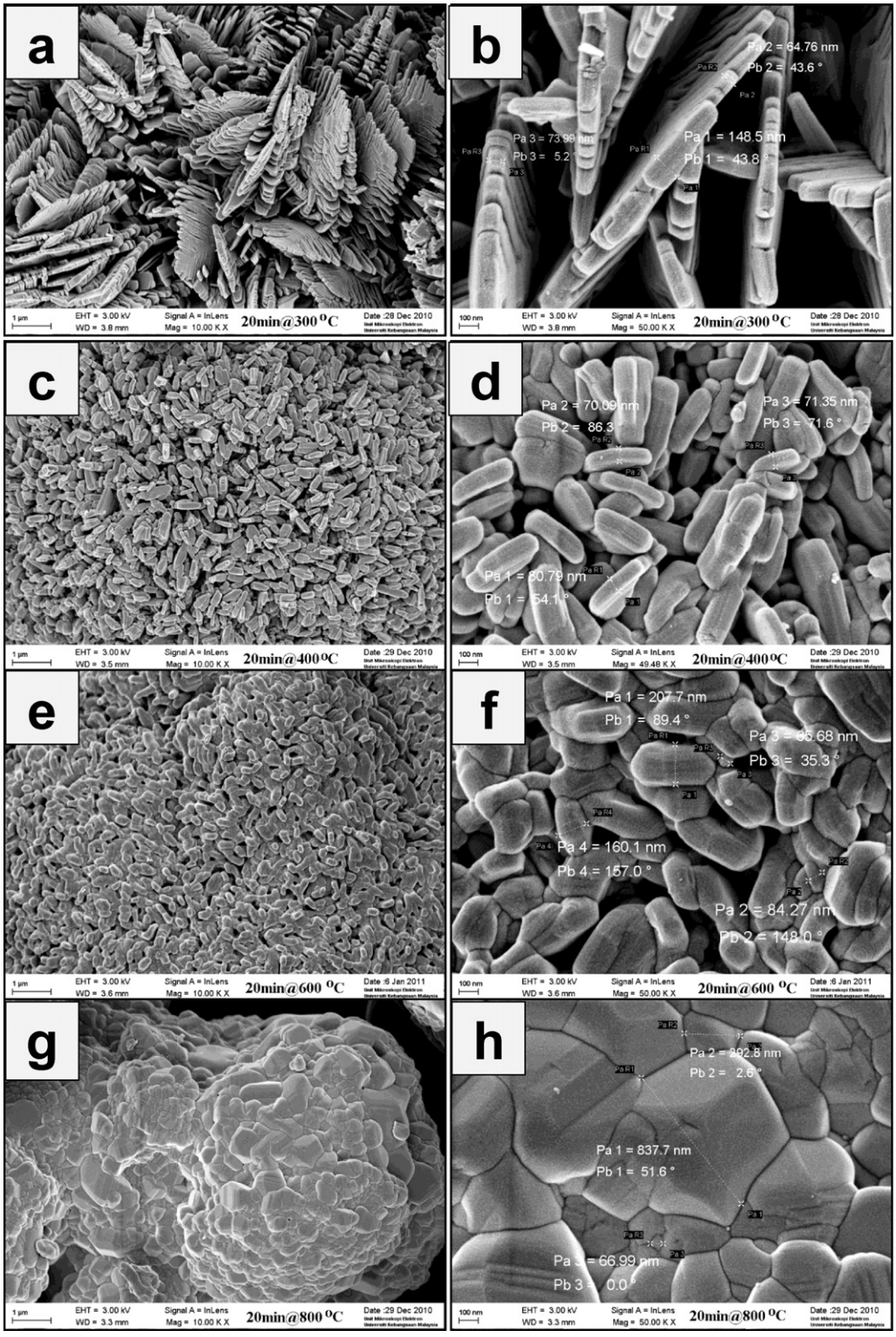

Fig. 2. The FESEM images of the CuO samples synthesized by rapid thermal decomposition of copper nitrate during 20 min at different temperatures, namely at 300 ((a) and (b)), 400 ((c) and (d)), 600 ((e) and (f)) and 800 °C ((g) and (h)).

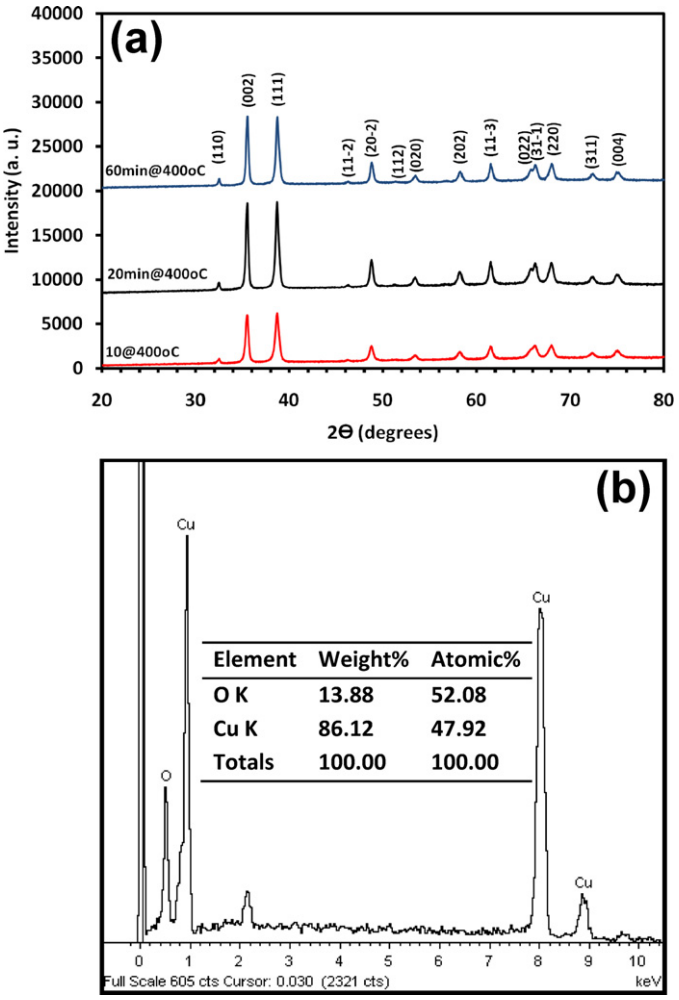

Fig. 3. (a) XRD patterns of all samples prepared by thermal decomposition of copper nitrate at 400 °C under atmospheric conditions during 10, 20 and 60 min and (b) the EDX spectrum of the rice-like CuO nanostructures prepared at 400 °C during 20 min.

3.1.2. Effect of the treatment time

The X-ray diffraction (XRD) patterns of the samples prepared at 400 °C with different treatment times namely 10, 20 and 60 min are shown in Fig. 3(a). All patterns correspond to CuO crystalline form with the base-centered monoclinic structure (JCPDS card no. 41-0254). Fig. 3(b) shows the energy dispersive X-ray spectroscopy (EDS) of the rice-like CuO nanostructures prepared at 400 °C during 20 min. Although EDS is not accurate in measuring the concentration of light elements such as oxygen and carbon, the results a ratio of Cu to O close to 1 for the rice-like nanostructures. All other prepared samples have similar EDS spectra.

Fig. 4 shows the FESEM images of the CuO nanostructures prepared at a fixed temperature (400 °C) during different times, namely 10 min (Fig. 4(a) and (b)), 20 min (Fig. 4(c) and (d)) and 60 min (Fig. 4(e) and (f)). From Fig. 4, we note that all samples have the same rice-like morphology of CuO with the grain size increasing as the treatment time increases.

3.2. Compositional analysis by XPS

The elemental composition and the oxidation state of the elements of the rice-like CuO nanostructures prepared at 400 °C during 20 min was analyzed by X-ray photoelectron spectroscopy (XPS). Fig. 5 shows the typical XPS spectra of the rice-like CuO nanostructures. Graph (a) is a typical XPS wide survey, (b) the typical high resolution XPS spectrum in the Cu 2p region, and graph (c) O 1s line of the rice-like CuO nanostructures. All peaks are indexed to Cu, O, and C as shown in Fig. 5(a) wide survey spectrum.

Fig. 5(b) demonstrates the Cu 2p core-level binding energy spectrum of the rice-like CuO nanostructures. The strong fitting peaks at around 933.4 and 953.4 eV are related to Cu^{2+} $2p_{3/2}$ and Cu^{2+} $2p_{1/2}$ peaks, respectively. However, the small fitting peaks at approximately 931.9 and 951.7 eV correspond to Cu^{1+} $2p_{3/2}$ and Cu^{1+} $2p_{1/2}$ peaks, respectively. This result indicates that the chemical valences of Cu at the surface of the rice-like CuO nanostructures are composed valence states of +1 and +2 [22]. The appearance of satellites (shake-up) peaks at about 940 and 960 eV (Fig. 5(b)) is fingerprint of the CuO phase with a d^9 electron configuration in ground state [23–25]. This is in agreement with the XRD and EDS results which indicate that the samples are pure CuO.

Fig. 5(c) shows the O 1s core-level spectrum which shows three different forms of oxygen. Three fitting Gaussians peaks marked as O1, O2 and O3 were used to fit the experimental data. Peak O1 (O 1s), positioned at the lower binding energy of 529.0 eV, is composed of O^{2-} in CuO [26,27]. The other two peaks O2 and O3 located at 530.6 and 532.0 eV are related to OH groups and H_2O absorbed onto the surface of the rice-like CuO nanostructures, respectively [28]. Peak positions or binding energy (BE) in eV for the core levels Cu 2p and O 1s relative to C 1s (284.5 eV) and their corresponding full-width at half maximum (FWHM) along with the respective atomic concentrations are listed in Table 3. The results show the ratio Cu/O is slightly lower than unity. However, it has to be pointed out that XPS probes the top surface layers (about 5 nm corresponding to three times the mean inelastic free path of the photoelectrons). The presence of three different oxygen species observed in the O1s spectrum indicates that the surface is oxygen enriched. However, the low values of the indirect gap suggest that the samples include significant amount of defects that could explain such copper deficiency of CuO samples.

3.3. Optical properties

UV–vis absorption spectroscopy technique has been used to study the optical absorption of the samples. The optical band gap energy (E_g) was estimated using the following equation [29,30]:

$$(\alpha h\nu)^n = B(h\nu - E_g) \quad (3)$$

in which α is the absorption coefficient, $h\nu$ is the photo energy, n equals either 1/2 for an indirect transition (indirect band gap semiconductors) or 2 for a direct transition (direct band gap semiconductors) and B is a material-dependent constant. The value of the absorption coefficient can be determined by the following equation [31]:

$$\alpha = \frac{-1}{d}\ln\frac{I_t}{I_o} = \frac{A}{d\log e} \approx 2.303\frac{A}{d} \quad (4)$$

where d is the thickness of the used cuvette (the sample thickness), I_o and I_t are the intensities of incident and transmitted light, respectively, $A = log(I_o/I_t)$ is the absorbance, obtained from the UV–vis absorption spectra.

The UV–vis absorption and reflectance spectra at room temperatures of the CuO samples prepared at different temperature (300, 400, 600 and 800 °C) during fixed time (20 min) are shown in Fig. 6(I) and (III), respectively. The UV–vis absorption and reflectance spectra of the samples prepared at fixed temperature (400 °C) during different times (10, 20 and 60 min) are shown in Fig. 6(II) and (IV), respectively. The typical optical absorption

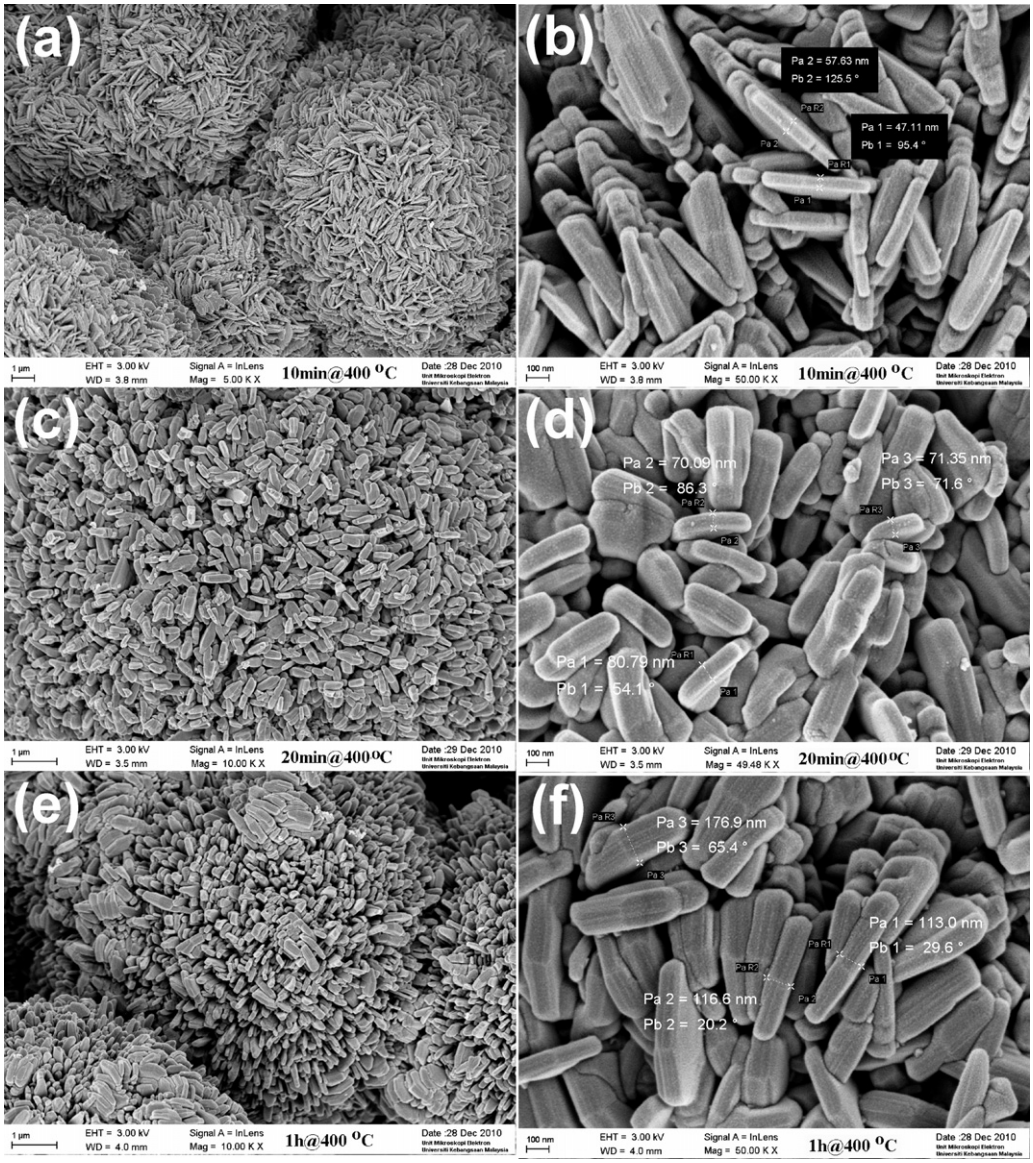

Fig. 4. The FESEM images of the CuO samples synthesized by rapid thermal decomposition of copper nitrate at 400 °C under atmospheric conditions during 10 min ((a) and (b)), 20 min ((c) and (d)) and 60 min ((e) and (f)).

Table 3
Binding energy (BE) values (in eV) for the core levels Cu 2p and O 1s and their corresponding full-width at half maximum (FWHM) and atomic concentration (in %).

Peak	Position BE (eV) ±0.10 eV	FWHM (eV) ±0.20 eV	Relative intensity Raw area (cps eV)	Atomic conc. (%)
Cu^{1+} $2p_{3/2}$	931.9	2.14	11,003.8	8.5
Cu^{2+} $2p_{3/2}$	933.3	2.37	18,943.7	–
Cu^{2+} shake-up satellite	941.1	4.86	20,379.7	30.5
O 1s (O1)	529.0	1.006	5995.8	33.9
O 1s (O2)	530.6	1.410	2776.9	15.7
O 1s (O3)	532.0	1.871	2011.9	11.4

spectra Fig. 6(I) and (II) show that there are three main absorption peaks; one of them is a sharp and strong absorption peak at about 210 nm and other two absorption peaks are broad and weak absorption peaks at about 280 nm and 330 nm. The very strong absorption peaks at about 210 nm (5.9 eV) could be related to the quartz cuvette.

The direct band gap energy of our samples was estimated by extrapolating the linear region at the steeply increasing curve of the plot of $(\alpha h\nu)^2$ on the y-axis against photon energy ($E = h\nu$) on the x-axis gives. The value of the gap is given by the x-intercept (as shown in Fig. 7(I) and (II)). The obtained values are also listed in Tables 1 and 2. Fig. 6(I) shows the estimated direct band gap energy of the CuO samples prepared during fixed time (20 min) at various temperatures (300, 600 and 800 °C). A systematic decrease of the direct band gap from 3.8 eV to 3.65 eV with increasing the treatment temperature from 300 °C to 800 °C can be observed in Fig. 6(I). From Fig. 6(II) and Table 2, the results indicate that the direct band gap of CuO nanostructures decreases from 3.5 eV to 3.18 eV as the treatment time increases from 10 to 60 min. The obtained direct band gap values (3.8, 3.7, 3.65 and 3.5 eV) are approximately identical with the results (3.87 and 3.72 eV) reported by Rehman et al. [32] and higher than the value (3.25 ± 0.05 eV) for bulk CuO reported by Koffyberg et al. [33]. The observed increase in of the direct band gap values (a blue shift) of CuO nanostructures may be associated with the decrease of the crystallite size.

Previous studies showed that CuO has an indirect gap ranging from 1.0 to 1.51 eV [32,34]. The value of the indirect gap can be estimated by plotting $(\alpha h\nu)^{0.5}$ against $(h\nu)$. However, it is quite difficult to obtain reliable values using this method because of the weak optical absorbance in the low energy range. However, it is possible to use the diffuse reflectance data to estimate the indirect gap as shown in Ref. [32]. The diffuse reflectance R can be used to define a function $F(R)$, Kubelka–Munk function [35], which is equivalent of the absorption coefficient in Eq. (3). $F(R)$ is given by:

$$F(R) = \frac{(1-R)^2}{2R} \tag{5}$$

The indirect band gap of CuO was estimated by plotting $(h\nu\ F(R))^{0.5}$ versus photon energy. The linear part of the curve was extrapolated to $(h\nu\ F(R))^{0.5} = 0$ to get the gap [32]. Using the data related to the sample prepared at $T = 400$ °C, 10 min, a value of 0.5 eV was obtained. This value is significantly lower than the value of bulk CuO (1.45 eV) reported by Gizhevskiĭ [36]. Rehman et al. [32] observed up to 0.25 eV red shift that they assigned to defects in the CuO nanostructures such as copper and oxygen vacancies. It is important to point out that the uncertainty on the obtained values for the indirect band gap is quite large because of the small range of photon energy used in fitting the experimental data. However, the results indicate clearly that the values of the indirect band gap of CuO nanostructures increase from 0.5 eV to 1.1 eV with the increase of the crystallite size from 28 nm to 48 nm as shown in Fig. 7(III) and Tables 1 and 2. The lower values could be related to the presence of high concentration of defects as suggested in [32].

The variation of the direct and indirect energy band gaps with the crystallite size was shown in Fig. 7(III) and (IV) and Fig. 8(III). Within the same conditions, increasing temperature (Fig. 7(III)) or time (Fig. 7(IV)), the direct energy gap decreases as the crystallite size increases.

Fig. 9 illustrates the room temperature photoluminescence (PL) spectra for (I) the CuO samples prepared during fixed time (20 min) at various temperatures (300, 400, 600 and 800 °C) and (II) the CuO samples prepared at fixed temperature (400 °C) during different times (10, 20 and 60 min). Generally, all CuO samples have similar PL spectra, which have three main broad emission

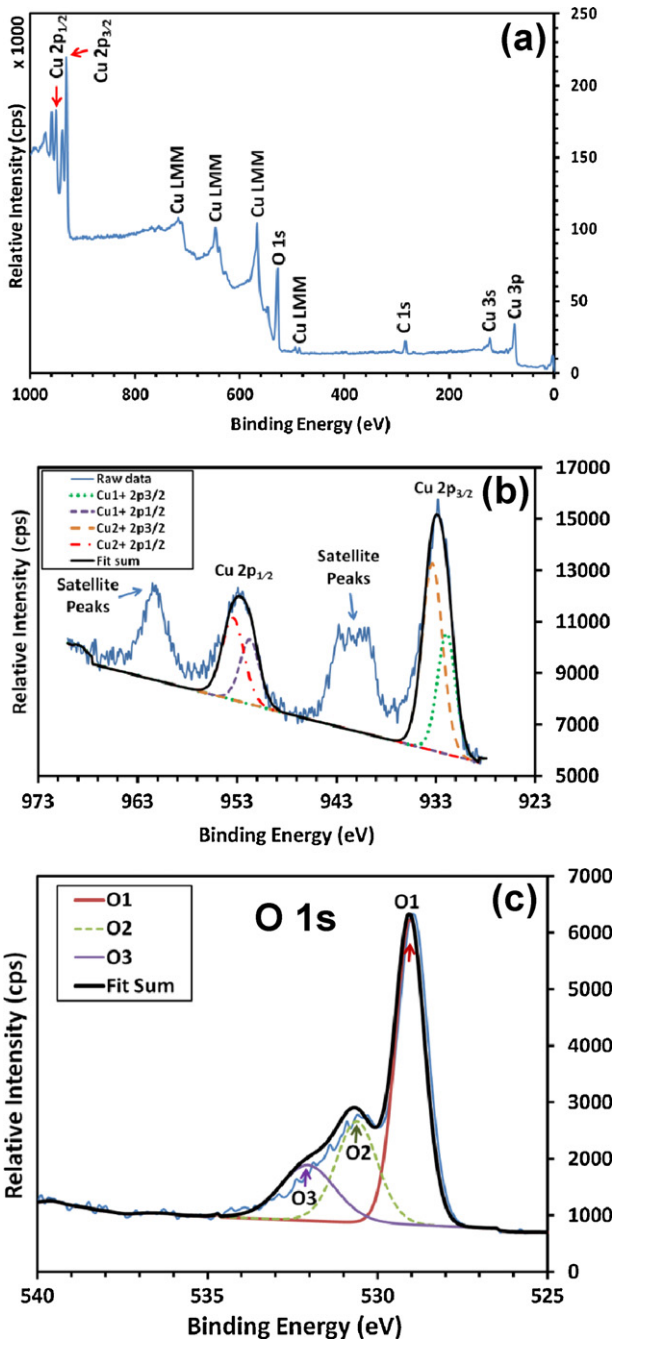

Fig. 5. XPS spectra of the rice-like CuO nanostructures prepared by thermal decomposition of copper nitrate at 400 °C during 20 min. Graph (a) is a typical XPS wide survey, graph (b) is the typical high resolution XPS spectrum in the Cu 2p region, and graph (c) O 1s region of XPS of the rice-like CuO nanostructures.

bands centered at about 305 nm (4.07 eV), 505 nm (2.46 eV) and 606 nm (2.05 eV). All emission bands with different peak wavelengths shown in Fig. 9 were previously reported for CuO [36–40]. The three strong emission peaks located at 489 (2.54 eV), 505 (2.46 eV) and 525 nm (2.37 eV) are due to the band edge emission from Γ_1^+ to the new sublevels at 300 K [41–45], or maybe due to the defects present in the CuO nanostructures [46]. The sub-levels could be developed because of imperfection levels due to the interaction of two excitons or the ^3D–^1D splitting in $Cu^+(3d^9 4s^2)$ [41,43]. Generally, the green emission bands extending from 489 nm (2.54 eV), 525 nm (2.37 eV) and 585 nm to 625 nm

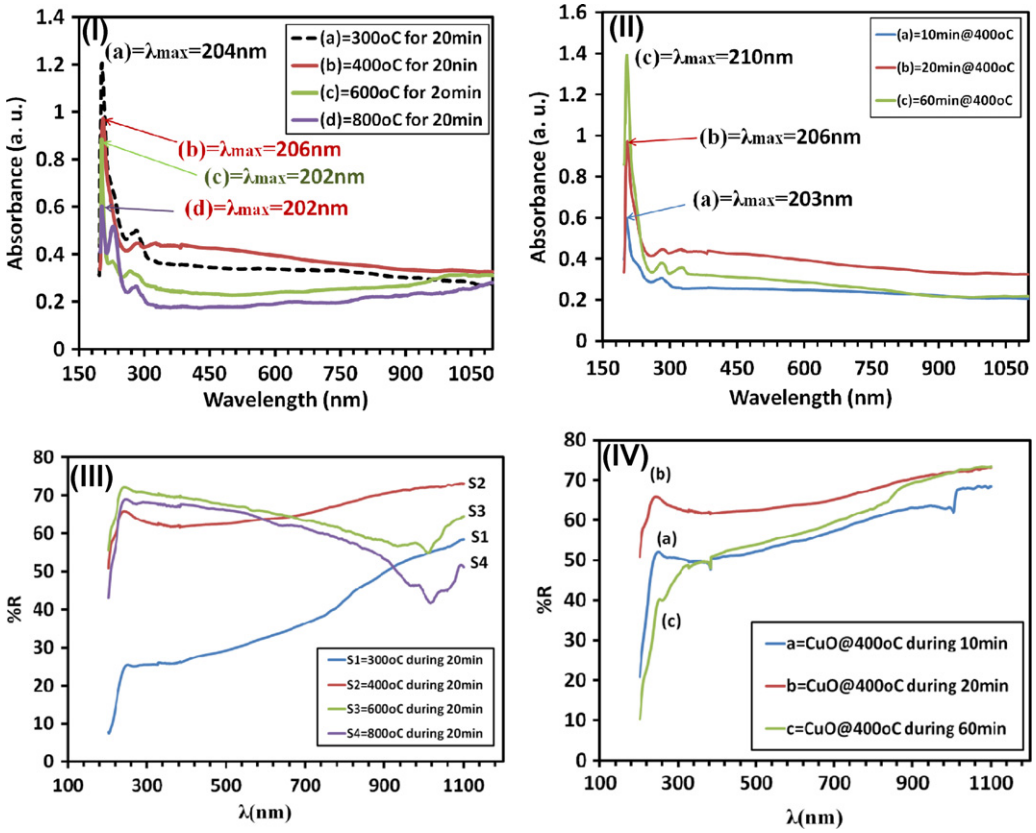

Fig. 6. The UV–vis absorption ((I) and (II)) and reflectance ((III) and (IV)) spectra at room temperatures of all CuO samples.

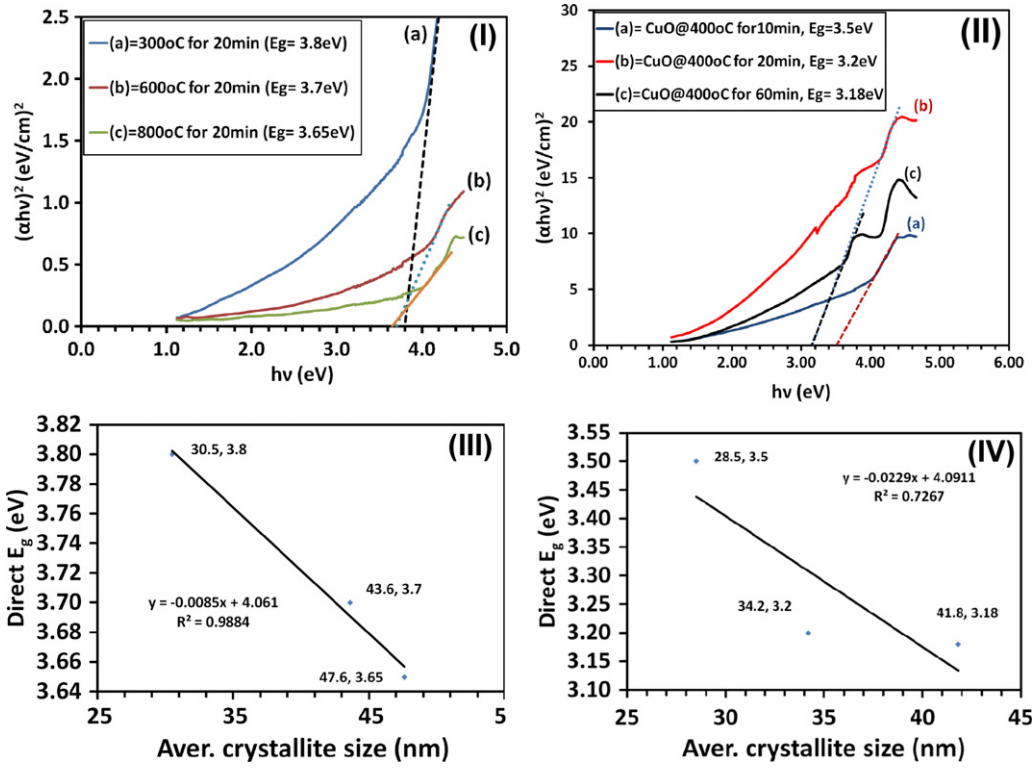

Fig. 7. (I) and (II) are direct band gap estimation of all CuO samples. Plot (III) and (IV) are the variation of the direct band gap with crystallite sizes.

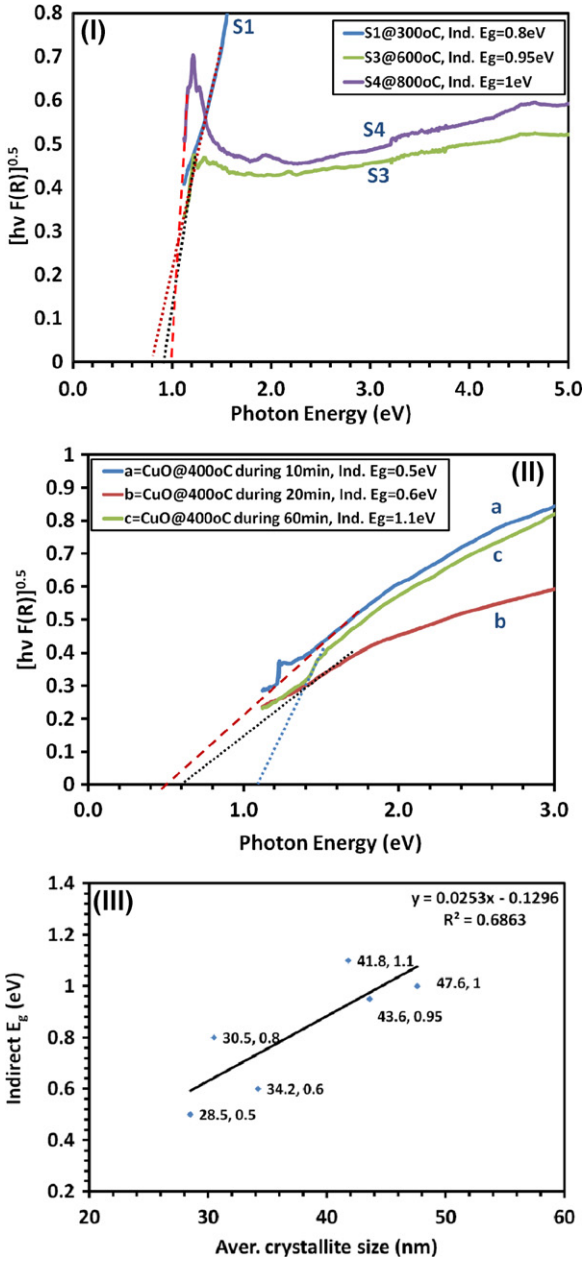

Fig. 8. (I) and (II) are indirect band gap estimation of all CuO samples. Plot (III) is the variation of the indirect band gap with crystallite sizes.

(1.99 eV) are related to deep level defects of CuO [37,39]. A significant increasing photoluminescence (PL) intensity at the emission band centered at about 505 (2.46 eV) was observed (Fig. 9). This PL emission decreases with the further increase of the temperature treatment from 300 °C to 800 °C (S1–S4 as shown in Fig. 9 (I)). At thermal decomposition temperature of 300 °C, the maximum intensity of the peak centered at 525 nm (2.37 eV), sample S1 (Fig. 9(I)) and (Fig. 9(II)) was obtained. This suggests that the thermal decomposition temperature of 300 °C is an optimum condition for the formation of CuO. The observed increase of PL intensity of the 305 nm (4.07 eV) band with the increase of the temperature treatment (Fig. 9(I)) is due to the enhancement of the crystallinity [36].

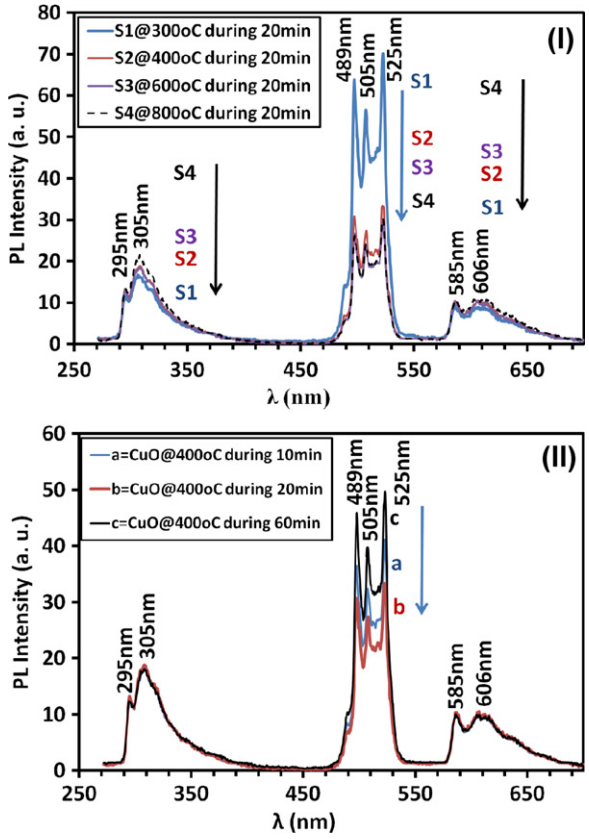

Fig. 9. Photoluminescence (PL) spectra of all CuO samples synthesized by rapid thermal decomposition of copper nitrate.

4. Conclusion

CuO nanostructures as a powder was produced by one-step thermal decomposition of copper nitrate within a short time (10 min). This novel method has many advantages compared to other methods such as simple, cheap and rapid (efficient in time). In addition, the products obtained by this new method do not need additional treatments such as washing and drying. The products have a high purity and quality. It is expected that the new thermal decomposition method could be used at an industrial scale as a simple, cheap and rapid technique in manufacture CuO and other metal oxides nanostructures with a high quality, purity and low cost. The preliminary results showed that the use of this new method can be extended further to prepare various metal oxides.

Acknowledgments

The authors would like to thank Universiti Kebangsaan Malaysia (UKM) for supporting this work through grant no: UKM-GUP-NBT-08-27-106 and UKM-AP-NBT-15-2010.

References

[1] U. Bjoerksten, J. Moser, M. Gratzel, Chem. Mater. 6 (1994) 858.
[2] Y. Jiang, S. Decker, C. Mohs, K.J. Klabunde, J. Catal. 180 (1998) 24.
[3] M. Frietsch, F. Zudock, J. Goschnick, M. Bruns, Sens. Actuators B 65 (2000) 379.
[4] R. Al-Gaashani, S. Radiman, N. Tabet, A. Razak Daud, Mater. Chem. Phys. 125 (2011) 846.
[5] E. Comini, C. Baratto, G. Faglia, M. Ferroni, A. Vomiero, G. Sberveglieri, Prog. Mater. Sci. 54 (2009) 1.
[6] B.J. Hansen, G. Lu, J. Chen, J. Nanomater. 2008 (2008) 830474.
[7] F. Marabelli, G.B. Parravicini, F. Salghetti-Drioli, Phys. Rev. B 52 (1995) 1433.
[8] G. Malandrino, G.G. Condorelli, G. Lanza, I.L. Fragala, J. Alloys Compd. 251 (1997) 314.
[9] T. Jarlborg, Physica C 454 (2007) 5.

[10] B.L. Chen, N. Lu, M.C. Xu, C.H. Yu, H.T. Wang, Electrochim. Acta 54 (2009) 4198.
[11] H. Wang, Q. Pan, J. Zhao, W. Chen, J. Alloys Compd. 476 (2009) 408.
[12] B. Liu, H.C. Zeng, J. Am. Chem. Soc. 126 (2004) 8124.
[13] H.-Y. Dang, Y.-L. Zhang, J.-K. Liang, S.-S. Xie, J. Mater. Sci. 28 (1993) 5176.
[14] W.Z. Wang, Y.J. Zhan, X.S. Wang, Y.K. Liu, C.L. Zheng, G.H. Wang, Mater. Res. Bull. 37 (2002) 1093.
[15] T. Kakihata, K. Usami, H. Yamamoto, J. Shibata, Technol. Rep. Kansai Univ. 40 (1998) 67.
[16] R.V. Kumar, R. Elgamiel, Y. Diamant, A. Gedanken, J. Norwig, Langmuir (2001) 1406.
[17] H. Wang, J.Z. Xu, J.J. Zhu, H.Y. Chen, J. Cryst. Growth 244 (2002) 88.
[18] Z.H. Liang, Y.J. Zhu, Chem. Lett. 33 (2004) 1314.
[19] C. Xu, Y. Liu, G. Xu, G. Wang, Mater. Res. Bull. 37 (2002) 2365.
[20] X. Zhang, D. Zhang, X. Ni, J. Song, H. Zheng, J. Nanopart. Res. 10 (2008) 839.
[21] F. Bakhtiari, E. Darezereshki, Mater. Lett. 65 (2011) 171.
[22] D. Gao, J. Zhang, J. Zhu, J. Qi, Z. Zhang, W. Sui, H. Shi, D. Xue, Nanoscale Res. Lett. 5 (2010) 769.
[23] J. Ghijsen, L.H. Tjeng, Phys. Rev. B 38 (1988) 11322.
[24] Y. Xiong, Z. Li, Y. Xie, J. Phys. Chem. B 107 (2003) 3697.
[25] W.-T. Yao, S.-H. Yu, Y. Zhou, J. Phys. Chem. B 109 (2005) 14011.
[26] J. Xu, W. Ji, Z. Shen, S. Tang, X. Ye, J. Solid State Chem. 147 (1999) 516.
[27] M.A. Dar, Q. Ahsanulhaq, Y.S. Kim, J.M. Sohn, W.B. Kim, H.S. Shin, Appl. Surf. Sci. 255 (2009) 6279.
[28] R.A. Zarate, F. Hevia, S. Fuentes, V.M. Fuenzalida, A. Zúñiga, J. Solid State Chem. 180 (2007) 1464.
[29] J. Pankove, Optical Processes in Semiconductors, Prentice-Hall, Englewood Cliffs, New Jersey, 1979.
[30] K.F. Shan, I.B. Kim, X.G. Liu, F.Z. Liu, Y.J. Sohn, J.W. Lee, J. Appl. Phys. 95 (2004) 4772.
[31] A.D. Yoffe, Adv. Phys. 42 (2) (1993) 173.
[32] S. Rehman, A. Mumtaz, S.K. Hasanain, J. Nanopart. Res. (2010), doi:10.1007/s11051-010-0143-8.
[33] F.P. Koffyberg, F.A. Benko, J. Appl. Phys. 53 (1982) 1173.
[34] G. Papadimitropoulos, N. Vourdas, V.Em. Vamvakas, D. Davazoglou, Thin Solid Films 515 (2006) 2428.
[35] E.L. Simmons, Appl. Opt. 14 (1975) 1380.
[36] B.A. Gizhevskiĭ, Yu.P. Sukhorukov, A.S. Moskvin, N.N. Loshkareva, E.V. Mostovshchikova, A.E. Ermakov, E.A. Kozlov, M.A. Uĭmin, V.S. Gaviko, J. Exp. Theor. Phys. 102 (2006) 297.
[37] B. Toboonsung, P. Singjai, J. Alloys Compd. 509 (2011) 4132.
[38] (a) A. Aslani, V. Oroojpour, Physica B 406 (2011) 144;
(b) A. Aslani, Physica B 406 (2011) 150.
[39] C. Jin, K. Baek, S. Park, H.W. Kim, W.I. Lee, C. Lee, Solid State Commun. 150 (2010) 1812.
[40] S.-S. Chang, H.-J. Lee, H.J. Park, Ceram. Int. 31 (2005) 411.
[41] R.J. Elliott, Phys. Rev. 124 (1961) 340.
[42] S. Jana, P.K. Biswas, Mater. Lett. 32 (1997) 263.
[43] D.W. Snoke, A.J. Shields, M. Cardona, Phys. Rev. B 45 (1992) 11693.
[44] R. Rossetti, J.L. Ellison, J.M. Gibson, L.E. Brus, J. Chem. Phys. 80 (1984) 4464.
[45] P. Sharma, H.S. Bhatti, Mater. Chem. Phys. 114 (2009) 889.
[46] Z. Yang, C.-K. Chiang, H.-T. Chang, Nanotechnology 19 (2008) 25604.